Phase matrix for light scattering by concentrically stratified spheres: comparison of geometric optics and the "exact" theory

Yoshihide Takano* and Kuo-Nan Liou

Joint Institute for Earth System Science and Engineering, and Department of Atmospheric and Oceanic Sciences, University of California, Los Angeles, California 90095, USA

*Corresponding author: ytakano@atmos.ucla.edu

Received 28 April 2010; revised 7 June 2010; accepted 10 June 2010; posted 10 June 2010 (Doc. ID 127625); published 9 July 2010

We have developed a hit-and-miss Monte Carlo geometric ray-tracing program to compute the scattering phase matrix for concentrically stratified spheres. Using typical refractive indices for water and aerosols in the calculations, numerous rainbow features appear in the phase matrix that deviate from the results calculated from homogeneous spheres. In the context of geometric ray tracing, rainbows and glory are identified by means of their ray paths, which provide physical explanation for the features produced by the "exact" Lorenz–Mie theory. The computed results for the phase matrix, the single-scattering albedo, and the asymmetry factor for a size parameter of ~600 compared closely with those evaluated from the "exact" theory.

OCIS codes: 290.1090, 290.4020, 290.5855.

1. Introduction

An incident plane electromagnetic wave can be thought of as a bundle of separate rays or a flow of photons impinging onto a scattering particle when the ratio of particle size to the incident wavelength approaches infinity. In this case, each localized ray or photon can be traced geometrically using Snell's law when it hits a particle's boundary. Fresnel's formula and the rotation of incident planes can be followed for the evaluation of intensity and polarization of a light ray, which can undergo (1) external reflection, (2) two refractions, (3) a number of internal reflections, and (4) internal absorption, along a traversed path. Also, a ray passing by a particle is diffracted in a narrow forward lobe with the same amount of energy as the reflected and refracted ray, which results in the extinction cross section becoming twice the particle's geometric cross section, a concept referred to as the geometric-optics approximation [1]. We have applied this concept to light scattering by nonspherical and irregular ice particles [2,3].

To the best of our knowledge, the geometric-optics approach has not been applied to light scattering and absorption by inhomogeneous spheres, except the work of Lock *et al.* [4]. We have developed a geometric-optics (GO) program for a concentric sphere following a ray-tracing program, which is coupled with a hit-and-miss Monte Carlo method specifically for application to nonspherical particles [2,3]. Our objective is to provide the means to understand the features in the phase matrix that are produced by the more "exact" Lorenz–Mie solution.

We have organized this paper as follows. In Section 2, we outline the fundamental equations that are required for the computation of the geometric ray-tracing program for a two-layer sphere. Computed results are subsequently presented and discussed in Section 3 in terms of ray paths, including external reflection, two refractions, and internal reflections, and the mixing rule. Finally, a summary is given in Section 4.

0003-6935/10/203990-07$15.00/0

2. Geometric Ray-Tracing Method for a Concentrically Stratified Sphere

In the following, we outline the basic equations for the calculation of phase matrix within the context of geometric optics. The scattering phase matrix involving a group of homogeneous or inhomogeneous spheres with different sizes can be expressed by

$$\mathbf{P} = \begin{bmatrix} P_{11} & P_{12} & 0 & 0 \\ P_{12} & P_{22} & 0 & 0 \\ 0 & 0 & P_{33} & -P_{43} \\ 0 & 0 & P_{43} & P_{44} \end{bmatrix}. \tag{1}$$

The four independent phase matrix elements P_{ij} in the matrix are given by

$$P_{ij} = \sum_{\gamma}\sum_{n} \frac{p_{ij,n}}{p_{11,n}\sin\theta_n}, \tag{2}$$

where the first summation denoted by γ covers the cross-sectional area of a scattering particle, and the second summation is over the localized rays denoted by the subscript $n(=1,2,3,\ldots)$. $p_{ij,n}$ are phase matrix elements for a photon scattered at a direction defined by a scattering angle θ_n. Equation (2) denotes that the phase function P_{11} is proportional to the number of scattered photons per unit solid angle. Suppressing the subscript n, p_{ij} in Eq. (2) can be expressed in terms of a 2×2 amplitude matrix $S_{kl}(k,l=1,2)$ as follows:

$$p_{11} = \frac{1}{2}(M_2 + M_3 + M_4 + M_1), \tag{3}$$

$$p_{12} = \frac{1}{2}(M_2 - M_3 + M_4 - M_1), \tag{4}$$

$$p_{22} = \frac{1}{2}(M_2 - M_3 - M_4 + M_1), \tag{5}$$

$$p_{33} = S_{21} + S_{34}, \tag{6}$$

$$p_{44} = S_{21} - S_{34}, \tag{7}$$

$$p_{43} = D_{21} + D_{34}, \tag{8}$$

where

$$M_k = |S_k|^2, \tag{9}$$

$$S_{kl} = S_{lk} = (S_l S_k^* + S_k S_l^*)/2, \tag{10}$$

$$D_{kl} = -D_{lk} = (S_l S_k^* - S_k S_l^*)i/2. \tag{11}$$

In these equations, the asterisk denotes a complex conjugate number. A scattering matrix $\mathbf{S}_n$ of an nth ray can be expressed by a product of transmission $\mathbf{T}$, reflection $\mathbf{R}$, and rotation $\mathbf{P}$ matrices [5], combining geometric reflection–refraction and Fraunhofer diffraction contributions in the form ([2,3])

$$\mathbf{S}_n = \begin{cases} \mathbf{R}_1 & \text{for} n = 1 \\ \mathbf{P}_t \mathbf{P}_s \prod_q \left[\mathbf{T}_n \mathbf{P}_n \prod_{k=n-1}^{2} (\mathbf{R}_k \mathbf{P}_k) \mathbf{T}_1 \mathbf{P}_1 \right]_q \mathbf{P}_e & \text{for} n \geq 2 \end{cases}, \tag{12}$$

where

$$\mathbf{P}_k = \begin{bmatrix} \cos\phi_k & \sin\phi_k \\ -\sin\phi_k & \cos\phi_k \end{bmatrix}, \quad \mathbf{R}_k = \begin{bmatrix} R_{lk} & 0 \\ 0 & R_{rk} \end{bmatrix},$$
$$\mathbf{T}_k = \begin{bmatrix} T_{lk} & 0 \\ 0 & T_{rk} \end{bmatrix}. \tag{13}$$

In Eq. (13), ϕ_k denotes a rotational angle between an incident plane and the next incident plane; R_{lk}, R_{rk}, T_{lk}, and T_{rk} are Fresnel reflection and transmission coefficients; and $\mathbf{P}_t$, $\mathbf{P}_s$, and $\mathbf{P}_e$ are rotational matrices between two coordinate systems [5]. When $n-1$ is less than 2, the term $\prod_{k=n-1}^{2}(\mathbf{R}_k\mathbf{P}_k)$ is an identity matrix.

Next, we outline a ray-tracing procedure for a concentric sphere. As shown in Fig. 1, rays refracted into a concentric sphere can undergo an additional refraction into a core. After refraction into the core surface, a new ray-tracing procedure is performed until the

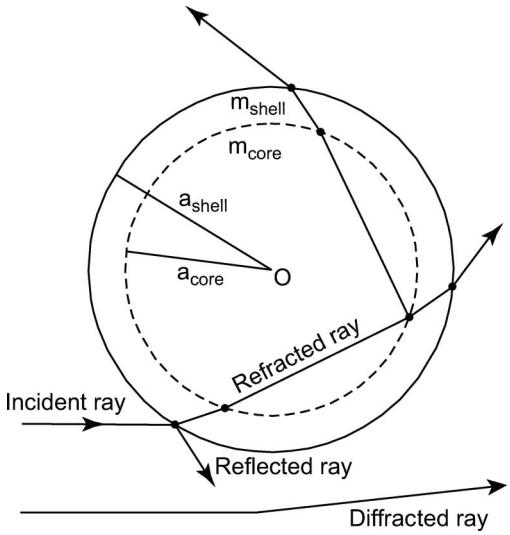

Fig. 1. Illustrative diagram for light scattering by a concentrically stratified sphere on the basis of the geometric ray-tracing approach.

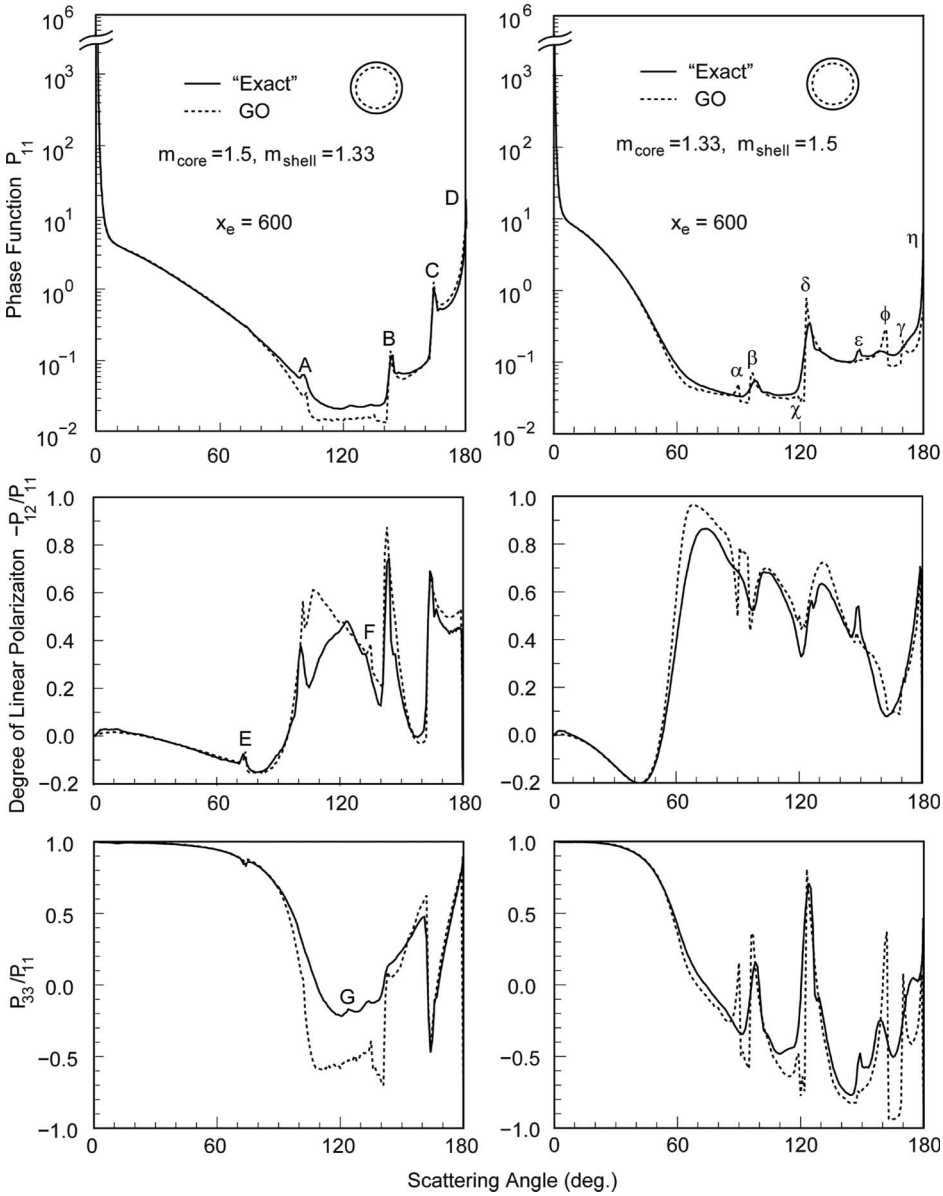

Fig. 2. Comparison of the phase matrix elements for polydisperse concentric spheres whose x_e is 600 between GO and the "Exact" Lorenz–Mie-like theory. Note that the matrix elements $P_{22} = P_{11}$ and $P_{44} = P_{33}$. The values for $P_{43} \sim 0$ and are not displayed here.

rays emerge out of the core. Subsequently, the preceding ray-tracing procedure is resumed in the shell portion of the system. This process is expressed symbolically by the product over q in Eq. (12) and repeated until the ray emerges out of the concentric sphere. Absorption in a concentric sphere is accounted for by considering whether a photon exists inside this sphere [3]. This is done by comparing the actual path length and the absorption path length defined by $-\ln \mathrm{RN}/k_i$, where RN is the random number from 0 to 1, $k_i = 4\pi m_i/\lambda$, m_i is the imaginary refractive index, and λ is the wavelength. The single-scattering albedo can be obtained from the ratio of the number of scattered photons to that of scattered photons if there were no absorption in a concentric sphere.

3. Computational Results and Discussion

We have carried out a comparison of the single-scattering properties for concentric spheres between GO and the "exact" computation (referred to as "Exact") to check the accuracy of the GO program. To smooth out the presentation of phase matrix elements, we perform a size integration using a modified gamma function $n(a)$, defined by

$$n(a) = Ca^{(1-3v_e)v_e} \exp\left(-\frac{a}{a_e v_e}\right), \tag{14}$$

where C is a constant, a is the radius of a sphere, a_e is the effective radius defined by

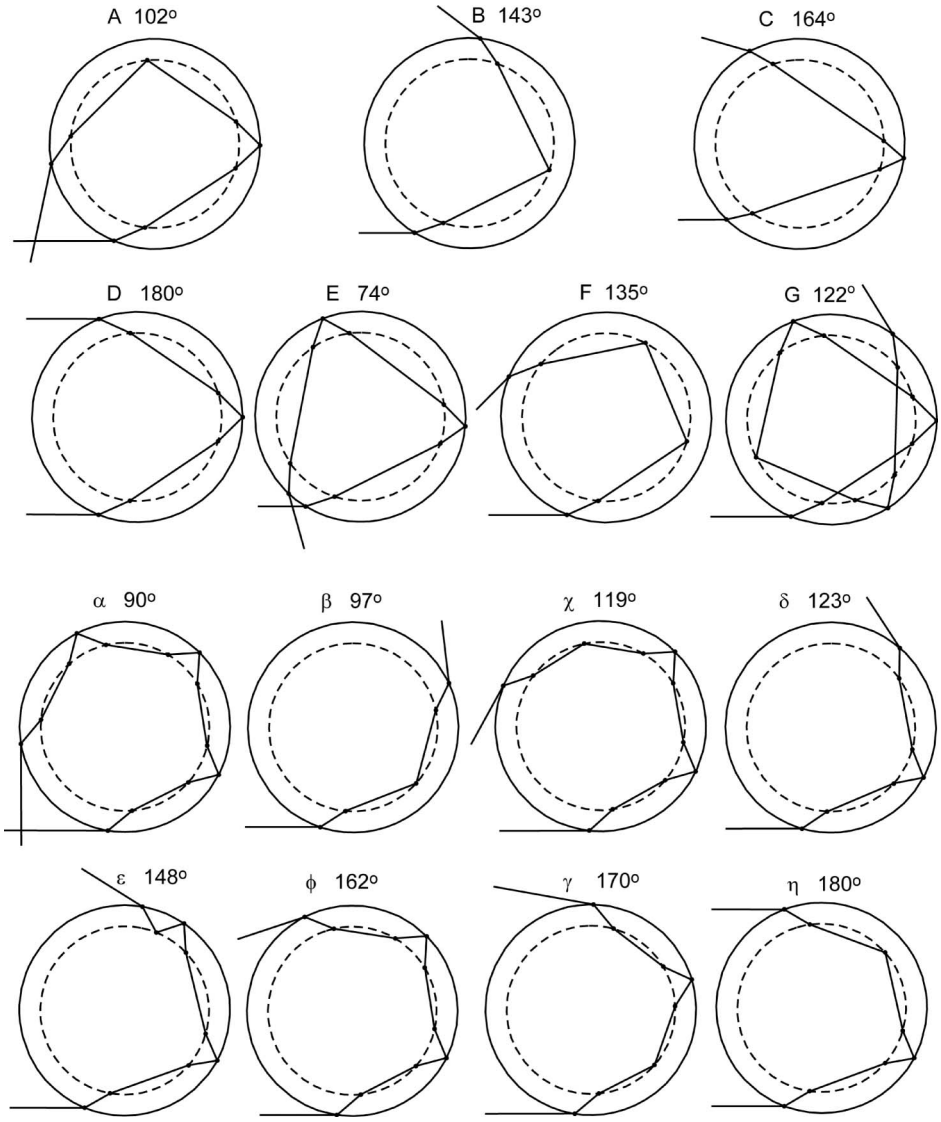

Fig. 3. Geometric rays that contribute to the production of rainbows and glory features, identified by alphabetical and Greek letters as shown in Fig. 2. The scattering angle for each case is also added beside the letter. The top two rows correspond to the left panel of Fig. 2, while the bottom two rows correspond to the right panel of Fig. 2.

$$a_e = \frac{\int a\pi a^2 n(a)\mathrm{d}a}{\int \pi a^2 n(a)\mathrm{d}a}, \tag{15}$$

and v_e is the effective variance given by

$$v_e = \frac{\int (a-a_e)^2 \pi a^2 n(a)\mathrm{d}a}{a_e^2 \int \pi a^2 n(a)\mathrm{d}a}. \tag{16}$$

For a concentric sphere, a_{shell} is substituted for a. For "Exact," we have followed the Lorenz–Mie-like code developed by Toon and Ackerman [6] and improved by Wiscombe [7]. These authors, as well as Kattawar and Hood [8], developed numerically stable algorithms for the spherical Bessel functions in the Lorenz–Mie solution based on the equations presented in [9].

Figure 2 shows the comparison of phase matrix elements for two concentric spheres between GO and "Exact" for an effective size parameter x_e of 600, where x_e is $2\pi a_e/\lambda$. This value for x_e is selected in expectation of the asymptotic approach of GO to "Exact" such that surface wave contributions to scattering and absorption are minimum. The effective variance v_e in this case is 1/9. The ratio of the core radius a_{core} to the shell radius a_{shell} is set as 0.8 for all sizes. In this figure, m_{core} and m_{shell} denote the refractive indices for the core and the shell of a concentric sphere, respectively. Rainbow and glory features are marked by alphabetical and Greek letters. For phase function P_{11}, GO and "Exact" results for Case 1 (left figure) and Case 2 (right figure) are reasonably close for all major features. For linear polarization $-P_{12}/P_{11}$, some deviation occurs in the region 100°–120° for Case 1 and 80°–90° for Case 2, where GO produces more features than "Exact." For the P_{33}/P_{11} element, differences are shown in the

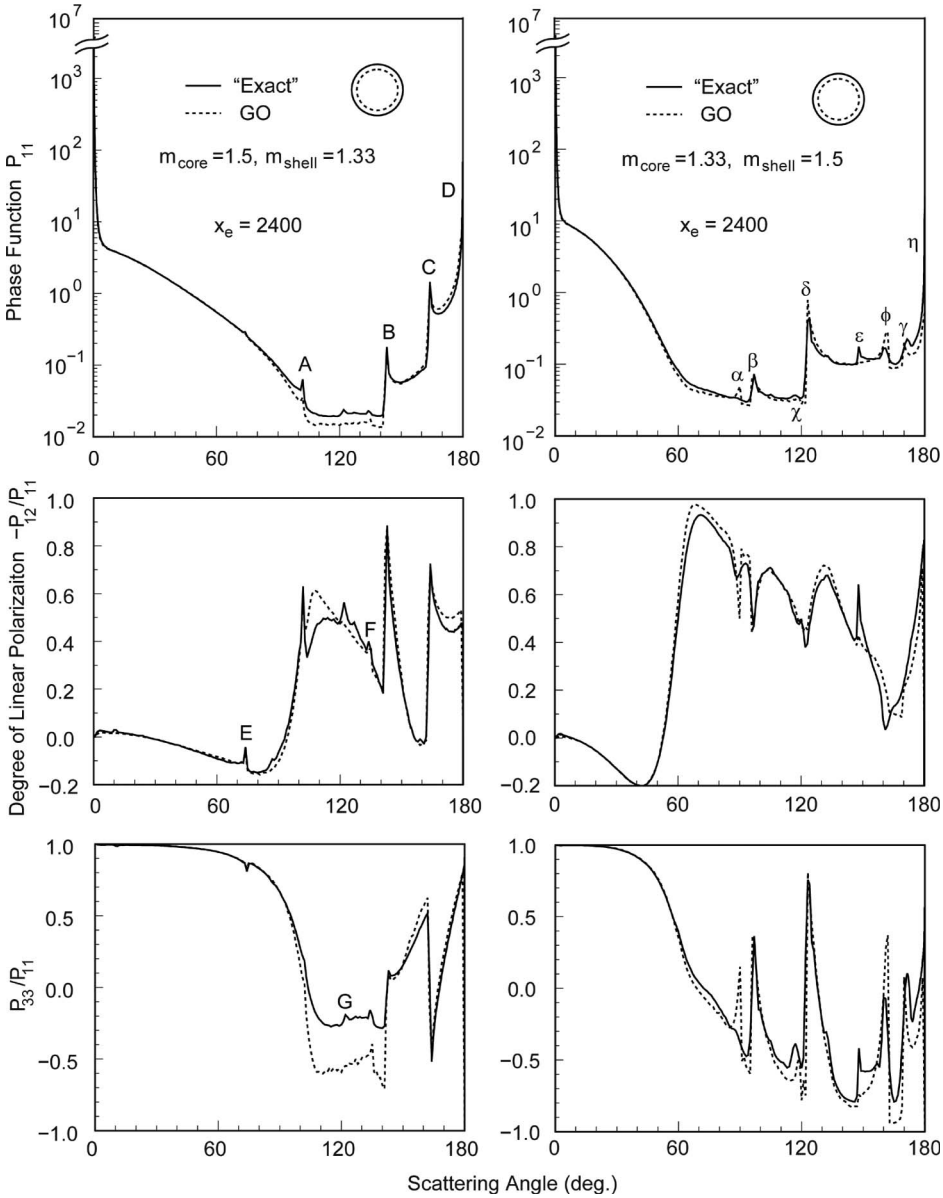

Fig. 4. Same as Fig. 2 except for $x_e = 2400$.

region 80°–120°. Values for the phase matrix element P_{43}/P_{11} are close to zero and are not presented here.

To understand the rainbow and glory features, we identify the rays that contribute to their production, as illustrated in Fig. 3. The most remarkable peaks *C* (primary rainbow) and *D* (glory) in Case 1 are generated by one internal reflection whose paths are modified by the shell structure. The other primary rainbow *B* is produced by internal reflection at the boundary between the core and the shell. Because of low reflectivity values of the inner sphere with a relative refractive index of 1.5/1.33, the intensity at *B* is smaller than that at *C* by one order of magnitude. Similarly, intensities of the compound secondary rainbow (reflections at both inner and outer spheres) *A* and the internal secondary rainbow *F* are weak. The weak secondary rainbow *E* appears only in the degree of linear polarization $-P_{12}/P_{11}$ and P_{33}/P_{11}, but not in the phase function because of the existence of intense twice-refracted rays in that region. Also, a very faint fourth-order rainbow *G* appears in P_{33}/P_{11}. For Case 2, the primary rainbow δ and glory η are most noticeable. In GO, the glory intensity *D* (Case 1) is larger than η (Case 2) by one order of magnitude due to an extra internal reflection in the latter. In "Exact," the intensity for glory η is about one third of that for glory *D*, probably due to the inclusion of surface wave contributions, which are not accounted for in the conventional geometric ray-tracing approach, as illustrated in Liou *et al.* [10]. The feature ϕ is the second intense rainbow, which does not occur clearly in "Exact" P_{11}. The secondary rainbow γ appears at the opposite side of the conventional secondary rainbows *A*, *E*, *F*, and ϕ because the maximum deviation angle becomes the minimum deviation angle in this case. In "Exact,"

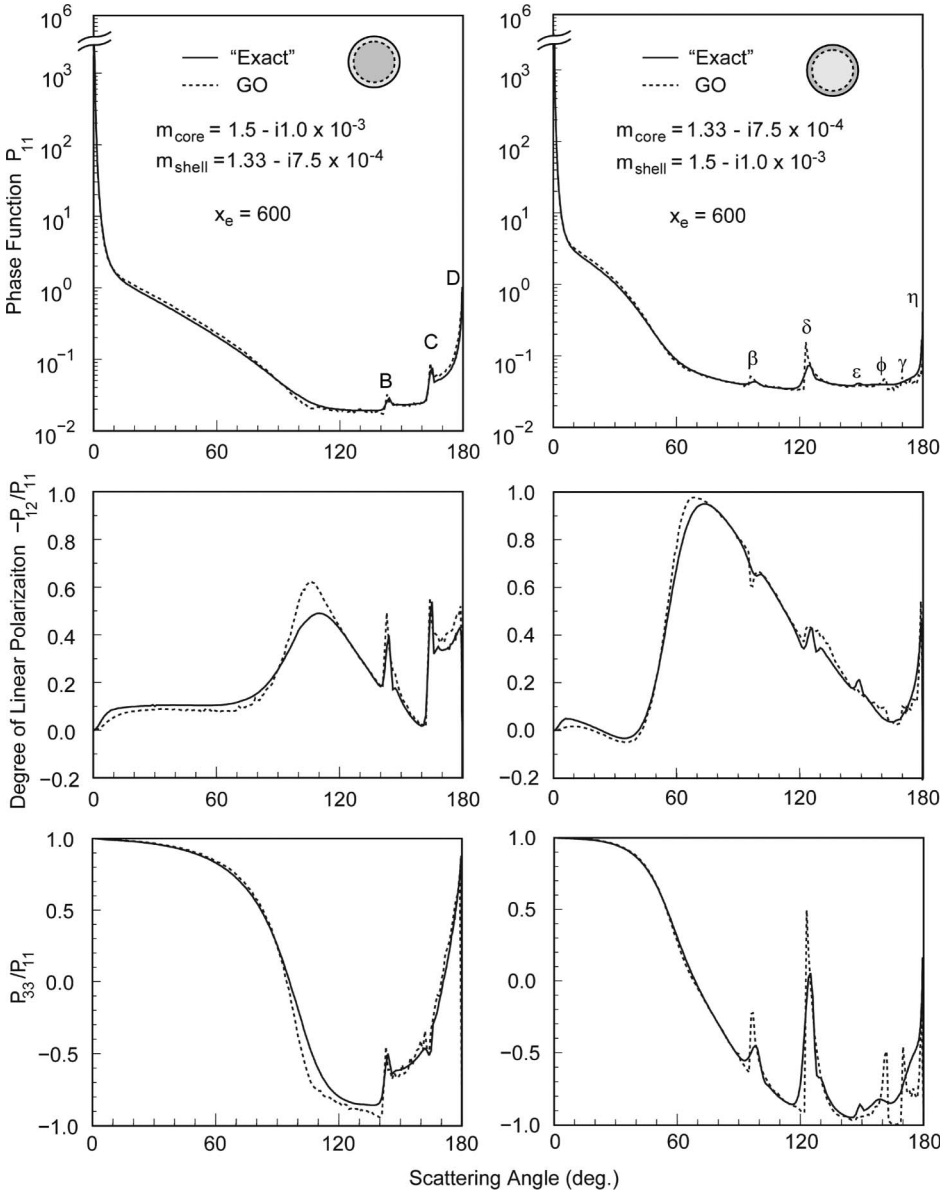

Fig. 5. Same as Fig. 2, except for $m_{\text{core}} = 1.5 - i1.0 \times 10^{-3}$ and $m_{\text{shell}} = 1.33 - i7.5 \times 10^{-4}$ in the left panel, and $m_{\text{core}} = 1.33 - i7.5 \times 10^{-4}$ and $m_{\text{shell}} = 1.5 - i1.0 \times 10^{-3}$ in the right panel.

there is no peak corresponding to γ; however, there is a faint peak around 175° in P_{33}/P_{11}. This peak would be closer to the GO peak if the size parameter is larger than 600. The third intense rainbow β is produced by one internal reflection. The remaining peaks α, χ, and ε are generated by external tertiary or compound tertiary reflections. As illustrated in Fig. 3, the external tertiary rainbow α is more pronounced than the compound tertiary rainbows χ and ε associated with intense reflection at the outer sphere. To clarify differences between GO and "Exact," such as α rainbow, we perform another comparison for a larger effective size x_e of 2400, which is shown in Fig. 4. "Exact" approaches GO much closer than that shown in Fig. 2. For example, "Exact" α rainbow appears in $-P_{12}/P_{11}$, although there is no α "Exact" rainbow in Fig. 2. Also, "Exact" ϕ and γ rainbows are more definitive than those depicted in Fig. 2. Additionally, the "Exact" G rainbow appears in $-P_{12}/P_{11}$. However, the fourth-order rainbow is not shown in GO. Differences in these features suggest that the "Exact" computer program developed by Toon and Ackerman [6] and Wiscombe [7] could partially contain issues for very large size parameters (see also Wolf and Voshchinnikov [11]).

Figure 5 shows three phase matrix elements as in Fig. 2, except that the imaginary refractive index is included for both core and shell. A number of rainbows (A, E, F, and α), which occur in Fig. 2, disappear due to accumulated absorption along the ray path inside the sphere. Energy contributions from the externally-reflected and two-refracted rays are more pronounced than the transmitted rays with internal reflection(s). For this reason, phase matrix elements

Table 1. Comparison of the Single-Scattering Albedo and Asymmetry Factor Computed from GO and "Exact" for a Combination of Real and Imaginary Refractive Indices Using x_e of 600

		Single-Scattering Albedo ϖ		Asymmetry Factor g	
m_{core}	m_{shell}	GO	Exact	GO	Exact
$1.5 - i2.0 \times 10^{-4}$	$1.33 - i1.5 \times 10^{-4}$	0.8611	0.8416	0.8588	0.8624
$1.33 - i1.5 \times 10^{-4}$	$1.5 - i2.0 \times 10^{-4}$	0.8841	0.8675	0.8924	0.8978
$1.5 - i1.0 \times 10^{-3}$	$1.33 - i7.5 \times 10^{-4}$	0.6183	0.6074	0.9331	0.9370
$1.33 - i7.5 \times 10^{-4}$	$1.5 - i1.0 \times 10^{-3}$	0.6565	0.6430	0.9333	0.9360
$1.4155 - i1.7559 \times 10^{-4}$	$1.4155 - i1.7559 \times 10^{-4}$	0.8721	0.8539	0.8783	0.8830
$1.4141 - i8.7298 \times 10^{-4}$	$1.4141 - i8.7298 \times 10^{-4}$	0.6360	0.6238	0.9343	0.9373

calculated from GO are in better agreement with those computed from "Exact" in absorbing cases than in nonabsorbing cases. Finally, we compare the single-scattering albedo and the asymmetry factor computed from GO and "Exact," as listed in Table 1. By adding different absorption values to the core and the shell of concentric spheres with an effective size parameter x_e of 600, we can examine the effects of concentric inhomogeneity on the single-scattering albedo. There is general agreement between GO and "Exact"; however, smaller differences are evident. To check these differences, we carried out an additional comparison using an average complex refractive index evaluated from the Maxwell–Garnett rule [12], which is listed in the bottom two rows. We see that the preceding differences are not produced by the inhomogeneity of scattering particles, but rather are caused by differences between GO and "Exact" in the homogeneous case. In reference to the asymmetry factor for nonabsorbing particles corresponding to Fig. 2, we obtain 0.8254 and 0.8236 for Case 1 and 0.8689 and 0.8728 for Case 2, respectively, for GO and "Exact." For absorbing cases listed in Table 1, agreement between the two is closely in line with the phase function values presented in 5.

4. Conclusions

Extending our previous geometric-optics approach for light scattering by nonspherical particles [2,3], we have developed a Monte Carlo/geometric ray-tracing program (GO) for the calculations of scattering, absorption, and polarization parameters involving a concentrically layered sphere. The phase matrix, single-scattering albedo, and asymmetry factor for concentric spheres are computed for a size parameter of ~600, using typical refractive indices for water and aerosols, and compared with those computed from the "Exact" Lorenz–Mie-like solution. In the derivation of the "Exact" solution [9], the matching of the boundary conditions for the tangential components of the electric field was performed at the core surface and the surface of the shell; as such, this solution was not directly derived from the wave equations. The shell-core system for spheres produces numerous rainbow and glory features, which differ substantially from those generated by homogeneous spheres. Based on the geometric ray-tracing principle, we have interpreted these imprints in GO and "Exact" in terms of the ray paths that undergo external reflection, two refractions, and internal reflections. Except for some weak rainbow features denoted by α, ε, and G displayed in Fig. 2, we see an overall agreement between GO and "Exact" for a size parameter of ~600. This agreement is enhanced for a size parameter of ~2400. We also note that differences in these two approaches could suggest that there appear to be unsolved problems in the "Exact" computational program for a two-layer spherical model for large size parameters.

This research was supported in part by the National Science Foundation (NSF) under grant ATM-0331550.

References

1. K. N. Liou, *An Introduction to Atmospheric Radiation*, 2nd Ed. (Academic, 2002).
2. Y. Takano and K. N. Liou, "Solar radiative transfer in cirrus clouds. Part I. Single-scattering and optical properties of hexagonal ice crystals," J. Atmos. Sci. **46**, 3–19 (1989).
3. Y. Takano and K. N. Liou, "Radiative transfer in cirrus clouds. III. Light scattering by irregular ice crystals," J. Atmos. Sci. **52**, 818–837 (1995).
4. J. A. Lock, J. M. Jamison, and C.-Y. Lin, "Rainbow scattering by a coated sphere," Appl. Opt. **33**, 4677–4690 (1994).
5. Y. Takano and K. Jayaweera, "Scattering phase matrix for hexagonal ice crystals computed from ray optics," Appl. Opt. **24**, 3254–3263 (1985).
6. O. B. Toon and T. P. Ackerman, "Algorithms for the calculation of scattering by stratified spheres," Appl. Opt. **20**, 3657–3660 (1981).
7. http://atol.ucsd.edu/scatlib/wiscombe.
8. G. W. Kattawar and D. A. Hood, "Electromagnetic scattering from a spherical polydispersion of coated spheres," Appl. Opt. **15**, 1996–1999 (1976).
9. M. Kerker, *The Scattering of Light and Other Electromagnetic Radiation* (Academic, 1969).
10. K. N. Liou, Y. Takano, and P. Yang, "On geometric optics and surface waves for light scattering by spheres," J. Quant. Spectrosc. Radiat. Transfer **111**, 1980–1989 (2010).
11. S. Wolf and N. V. Voshchinnikov, "Mie scattering by ensembles of particles with very large size parameters," Comput. Phys. Commun. **162**, 113–123 (2004).
12. C. F. Bohren and D. R. Huffman, *Absorption and Scattering of Light by Small Particles* (Wiley, 1983).